Historic contamination alters mercury sources and cycling in temperate estuaries relative to 1 2 uncontaminated sites Emily A. Seelen^{a*1}, Celia Y. Chen^b, Prentiss H. Balcom^{a,d}, Kate L. Buckman^b, Vivien F. Taylor^c, 3 Robert P. Mason^a 4 5 a. University of Connecticut, Department of Marine Sciences, 1084 Shennecossett Road, 6 Groton, CT, 06340 USA 7 b. Dartmouth College, Department of Biological Sciences, Hanover, NH 03755 USA c. Dartmouth College, Department of Earth Science, Hanover, NH 03755 USA 8 d. Harvard John A. Paulson School of Engineering and Applied Sciences (SEAS), 29 Oxford 9 10 Street, Cambridge, MA 02138 USA 11 12 seelen@usc.edu, celia.y.chen@dartmouth.edu, pbalcom@seas.harvard.edu, kate.l.buckman@dartmouth.edu, vivien.f.taylor@dartmouth.edu, robert.mason@uconn.edu 13 14 *Corresponding author: seelen@usc.edu 15 1. Present Address: University of Southern California Dornsife, Department of Earth Science, 16 17 3651 Trousdale Pkwy, Los Angeles, CA 90089 USA 18

Abstract

Mercury (Hg) is a global and persistent pollutant which can be methylated to more toxic forms (methylmercury; MeHg) in natural systems. Both forms pose a risk to humans and wildlife, and exposure often begins in aquatic environments. Therefore, quantifying aquatic concentrations and identifying source pathways is important for understanding biotic exposure. In this study, data from estuaries in the Northeast United States were combined to evaluate how point source contamination impacts the concentration and source dynamics of water column total and MeHg with an emphasis on sediment versus non-sediment sources. Partial least squares regression models were implemented to identify a set of variables most related to water column MeHg and total Hg (HgT) across the estuaries. The main findings suggest that contaminated sites have strong internal recycling of HgT that dominates over external inputs, and this leads to elevated concentrations of HgT and MeHg in the local water columns. However, HgT sources in uncontaminated estuarine systems have a strong connection to the local watershed with dissolved HgT linked to dissolved organic carbon, and particulate HgT linked to watershed land use and estuarine mixing. There was little correlative evidence that water column MeHg concentrations were linked to sediment in such systems, but unlike HgT, the concentrations were also not clearly linked to the watershed. Instead, in situ methylation of dissolved water column HgT appeared to dominate the MeHg source pathway. The results suggest that Hg point-source contaminated sites should be considered independently from non-contaminated sites in terms of management, and that land use plays an important indirect role in coastal MeHg dynamics.

40

20

21

22

23

24

25

26

27

28

29

30

31

32

33

34

35

36

37

38

41 Keywords: Mercury; Methylmercury; Coastal Systems; Contamination; Multi-Estuary Analysis;

Source Dynamics

Abbreviations: Mercury, Hg; Methylmercury, MeHg; Total mercury, HgT; Inorganic Hg, Hg^{II};
Dissolved organic carbon, DOC; Principal component analysis, PCA; Partial least squares
regression model, PLSRM; High organic carbon, HOC; Low organic carbon, LOC; Supporting
information, SI; Hydrological unit code, HUC; Particulate MeHg, pMeHg; Dissolved MeHg,
dMeHg; Particulate HgT, pHgT; dissolved HgT, dHgT; Bromine monochloride, BrCl; Chlorophyll
a, chl a; phaeopigment, pha; Percent loss on ignition, %LOI; Partition coefficient, Kd; Variable

1. Introduction

influence on projection, VIP

Mercury (Hg) primarily exists as three intrinsically linked forms in the environment; inorganic Hg (iHg^{II}) is the major parent species for methylmercury (MeHg) formation (Lexmond et al., 1976), and iHg^{II} is mostly deposited to ecosystems post atmospheric Hg⁰ oxidation (Lyman and Jaffe, 2012; Obrist et al., 2011b; Outridge et al., 2018). Point sources of iHg^{II} from industrial activity are also significant in some areas (Hsu-Kim et al., 2018; Kocman et al., 2013). The most toxic form of Hg in the environment is MeHg due to its heightened propensity to bioaccumulate (Mason et al., 2012; Sunderland, 2007). The net transformation of iHg^{II} to MeHg within, and delivery of MeHg to, coastal water columns controls the levels of MeHg exposure to aquatic

biota (Chen et al., 2014) and humans (Selin et al., 2010; Sunderland, 2007). Therefore, understanding how atmospheric/watershed sources and historic Hg point contamination impact coastal water column MeHg concentrations is important for understanding exposure under those different conditions. However, the complicated formation, transport, and degradation dynamics of MeHg combined with its strong relationship to Hg^{II} and dissolved organic carbon (DOC) (Bergamaschi et al., 2012; Grigal, 2002; Mitchell et al., 2012; Stoken et al., 2016; Taylor et al., 2019; Turner et al., 2018) make identifying sources of MeHg in estuarine water columns challenging. Studies such as Balcom et al. (2015) and Jiang et al. (2017) have shown that contaminated sites do not follow Hg patterns observed in non-contaminated sites, but Taylor et al. (2019) showed that even when comparing only uncontaminated sites MeHg-HgT-OC relationships are not consistent. Therefore, single correlation analyses do not give enough information towards the relative importance of multiple stressors that simultaneously influence HgT and MeHg concentrations in coastal systems. For this study, we utilized a multivariate, multi-watershed approach in order to overcome these limitations. Multi-watershed Hg source analyses are useful as they allow for the isolation of potentially universal ecosystem parameters predictive of MeHg concentrations rather than those which may be site specific. Multi-watershed analyses are used less frequently than single system studies but have been employed in different areas around the world (Balcom et al., 2015; Bravo et al., 2018; Chen et al., 2014; Driscoll et al., 2012; Grigal, 2002). For example, a latitudinal study in Europe (Bravo et al., 2018) led the authors to observe a pattern of elevated %MeHg in streams high in sulfate and autochthonous DOM, suggesting that MeHg production is in situ but tied to watershed land use. Balcom et al. (2015) focused on estuarine sediment MeHg sources.

61

62

63

64

65

66

67

68

69

70

71

72

73

74

75

76

77

78

79

80

81

They found that sediment alone cannot predict water column MeHg across sites sampled from the Northeastern United States, but the two compartments were linked at sites with high turbidity or historic contamination. They also observed tidal differences in MeHg concentrations at single sampling locations which they interpreted as being due to watershed inputs. However, their study lacked indices of in situ carbon levels and watershed land use that limited their data interpretation (Balcom et al. 2015). Understanding the relative importance of external inputs compared to internal processes provided the motivation for the analysis described here. The overarching aim of this study was to examine the impact of human activity on the concentration and sources of estuarine water column MeHg, with a focus on the importance of historic Hg contamination and watershed land use. The study combines four years' worth of sediment, water column, and local watershed land use data from ten estuarine systems in the Northeast United States to answer three main questions: 1) Do the sources and controls on water column Hg and MeHg differ in Hg contaminated sites from non-contaminated sites? 2) When is sediment the dominant source of MeHg to coastal waters? and 3) Is there a common set of predicting variables for water column MeHg and Hg across a range of temperate estuaries? It is recognized that most earth systems have some degree of Hg contamination from atmospheric inputs and other remote sources, but, for simplicity, we use "contaminated" in this text to refer to point source contaminated sites and "uncontaminated" to refer to sites where Hg inputs are dominated by regional atmospheric Hg deposition. Correlation, principal component analysis (PCA), and partial least squares regression modeling (PLSRM) were tools used to visualize relationships in the data and select the statistically important drivers for water

83

84

85

86

87

88

89

90

91

92

93

94

95

96

97

98

99

100

101

102

103

column MeHg and total mercury (HgT) concentrations. The multi-estuary approach allowed us to identify key variables influencing the coastal Hg cycle, thus enhancing the understanding of the factors driving HgT and MeHg concentrations in estuarine waters.

2. Methods

105

106

107

108

109

110

111

112

113

114

115

116

117

118

119

120

121

122

123

124

125

126

2.1. Sampling locations

Water and sediment samples were collected from 10 estuarine ecosystems located along the northeast coast of the United States (Table 1, Fig. S1) between the years 2012 and 2016. Data from 2012 were previously published in Buckman et al. (2017) and the 2013 data in Taylor et al. (2018). The 2015 and 2016 data have not been previously published except for the process focused studies of Seelen et al. (2018) and Mazrui et al. (2016). Fifty-five data points consisting of forty-one unique sites were included (Table 1). The discrepancy in the total numbers is due to seasonal sampling that took place at 11 sites in 2016 and three overlapping sites in 2013 and 2015. All samples were collected between May and September. In 2013 and 2015, sites were selected along a latitudinal gradient with paired subsites of relatively high (HOC) and low (LOC) organic carbon sediment sampled in close proximity. These site designations were based on visual inspection (muddy versus sandy) rather than chemical analysis and so there are, for example, HOC sites in the Chesapeake Bay that have a lower %LOI than LOC sites in Maine (Table S2). Thus, this nomenclature reflects the differences between two sites in close proximity but not their sediment characteristics within the full dataset. In 2012 and 2016, the sites were selected along salinity gradients of three estuaries, the Delaware River (2012), Berry's Creek/Hackensack River (2016), and the Penobscot River Estuary (2016), with the latter two being mercury contaminated sites (Table 1). More site details are provided

in Table 1, which includes an indication of the contaminated sites, and the full dataset is shown in the Supporting Information (Table S2). The site selection and timespan of sampling may be specific to the region and season, but the consistency of the results to previous studies suggests this approach is highly informative for future research.

2.2. Sample Collection

127

128

129

130

131

132

133

134

135

136

137

138

139

140

141

142

143

144

145

146

147

Samples were collected from shore or small boat by hand using clean sampling techniques and processed within 12 hours of collection. Water was filtered using either 550 °C combusted quartz fiber filters (2012, 2013, 2016) or sequentially filtered using 20 µm nylon filters and 0.2 μm polycarbonate filters cleaned with 2% hydrochloric acid (2015). The sequential filters were summed to calculate a bulk sample. The filters were stored frozen until analysis for the particulate HgT and MeHg datasets. Dissolved samples were collected after the quartz filter or 0.2 µm polycarbonate filter into acid cleaned iChem bottles and preserved with 0.2% HCl if intended for HgT or combined MeHg and HgT analyses. Samples for only dissolved MeHg were preserved with 0.5% H₂SO₄. DOC samples were collected from the particulate Hg filtrate into muffled amber vials and nutrient samples into acid cleaned plastic centrifuge tubes; both were preserved by freezing. DOC flocculation was not observed in the water samples after freezing. It is recognized that estuarine conditions change over a tidal cycle which may impact Hg cycling (e.g. Bergamaschi et al., 2012; Pato et al., 2010). For this analysis, samples collected at high tide were favored. When a high tide sample was not available samples collected at rising tide were used (22% at rising tide in the Full Model with all sites included, 13% in the Reduced Model with the contaminated sites removed) (Table S2). The sediment sampling was conducted using a

push core or a surface grab sample with the top <4 cm considered as the surface. Sediment was collected sub-tidally near low tide, processed, and stored frozen. They were then freeze dried and homogenized prior to analysis. Between 2 and 9 sediment field replicates from a small area were collected per location and averaged for the statistical analysis. The years with more samples collected, 2015 and 2016, had slightly higher sample variance. For example, sites with n=3 sediment samples collected had an average of 30% variance in HgT concentrations whereas those with n>3 had 49% variance. However, in all cases the field replicates were collected in close proximity and the variance is similar to what has been found in other studies (e.g. (Bloom et al., 1999). The number of sediment samples collected and standard error for the sediment variables are given in Table S2. Water column field replicates were not collected, and therefore error is included only for the analyses.

Land cover for each site's sub-watershed was determined using hydrological unit code sub-watershed (HUC-12) delineations in GIS based on the 2011 National Land Cover Database. Land cover in the HUC-12 system includes open water, perennial ice/snow, developed open space, developed low intensity, developed medium intensity, developed high intensity, barren land, deciduous forest, evergreen forest, mixed forest, shrub/ scrub, grassland/ herbaceous, pasture/hay, cultivated crops, woody wetlands and emergent herbaceous wetlands. For this analysis, the open water fraction was removed from the percent calculations. No perennial ice/snow was observed so it was not included. Barren and grassland were also omitted due to low presence (average less than 1.2%). Land cover categories were summed to generate fewer variables: here developed low = developed open space and developed low intensity; developed high = developed medium and high intensity; forest = deciduous, evergreen, mixed forest, and

shrub/scrub; agriculture = pasture/hay and cultivated crops; and wetland = woody and emergent herbaceous wetlands. Catchment size was also determined using the HUC delineation. Average monthly rainfall was determined using the modelmywatershed.org website which sources data from PRISM Climate Data (PRISM Climate Group, 2019).

2.3. Sample Chemical Analysis

170

171

172

173

174

175

176

177

178

179

180

181

182

183

184

185

186

187

188

189

This section is specific to the 2015 and 2016 datasets. The 2012 and 2013 analysis descriptions can be found in Buckman et al. (2017) and Taylor et al. (2019), respectively. Particulate and dissolved MeHg (pMeHg and dMeHg, respectively) samples were analyzed on a Tekran 2700 Automated Methylmercury Analysis System following standard techniques (Hammerschmidt and Fitzgerald, 2006; Munson et al., 2014). Briefly, particulate samples were digested in 4.5N nitric acid overnight, neutralized with potassium hydroxide and acetate buffer, and ethylated using sodium tetraethylborate before separation by gas chromatography and cold vapor atomic fluorescence detection with calibration against a standard curve (Alfa Aesar CAS: 115–09–3, LOT: 1791821 spike recovery= 103±14%). Dissolved MeHg samples were analyzed similarly except the seawater was digested overnight in 1% H₂SO₄, and 2.5% L-ascorbic acid was added prior to ethylation (Munson et al., 2014) (Alfa Aesar CAS: 115–09–3, LOT: 1791821 spike recovery= 86±34%). The variability in the MeHg analysis is in part due to the variability when measuring low concentration samples; the samples were not corrected for spike recovery. MeHg was extracted from the bulk sediment via aqueous distillation (Hammerschmidt and Fitzgerald, 2001) and analyzed on the Tekran 2700, as described above (Alfa Aesar CAS: 11509–3, LOT: 1791821 spike recovery= 114±8%). The methods are a modified version of EPA method 1630.

HgT was analyzed on a Tekran 2600 by cold vapor atomic fluorescence spectrometry following EPA method 1631, refined by Hammerschmidt and Fitzgerald (2006). The particulate HgT (pHgT) sample filters were digested in 4.5N nitric acid with bromine monochloride (BrCl) for 16 hrs, followed by hydroxylamine hydrochloride and stannous chloride additions before analysis. Calibration was against a standard curve and the results were spike corrected (J.T.Baker CAS: 7732–16–5, Batch No: 0000127949 spike recovery= 121±2%). For some samples, the same filter was used for both pMeHg and pHgT, in which case the BrCl addition was made after the MeHg analysis was complete. Dissolved HgT (dHgT) analysis was similar to the particulate analysis, except only BrCl was added >16 hr for digestion prior to reduction for analysis. The samples were blank and spike corrected (J.T.Baker CAS: 7732–16–5, Batch No: 0000127949 spike recovery= 76±5%). Bulk sediment HgT was analyzed via a direct mercury analyzer: a DMA-80 at Umeå University (ARC-CNRC MESS-3 CRM recovery= 101±2%), and a DMA-80 and MA 3000 at the University of Connecticut (PACS-3 CRM recovery= 103±1%), depending the year sampled (EPA method 7473).

Chlorophyll a (chl a) and phaeopigment (pha) concentrations were quantified from wet filters using fluorescence techniques after 90% acetone extraction and acidification for pha. DOC was analyzed on a Shimadzu TOC/TN analyzer (duplicate average RSD = 6.6% and 2.8%, respectively). Sediment bulk organic matter content was based on percent loss on ignition

(%LOI) when a known sample mass was burned for a minimum of 4 hours at 550°C (Dean, 1974).

2.4. Statistics

210

211

212

213

214

215

216

217

218

219

220

221

222

223

224

225

226

227

228

229

The dataset consisted of measured and calculated Hg variables (dissolved and particulate HgT and MeHg, sediment bulk HgT and MeHg, %MeHg and partition coefficients (Kd)), ancillary variables (salinity, temp, conductivity, pH, DO, DOC, TSS and sediment %LOI), watershed characteristics (latitude, catchment size, rainfall) and land use (31 total) (Table S1). Data gaps due to lost or damaged samples were filled with the data average of other samples taken for this study from nearby sites (for instance, the average of upstream and downstream sites). The missing values represented <5% of each variable and are noted in Table S2. Below detection limit values were replaced with half the detection limit, as described by EPA methods (EPA, 2000), which is valid when the BDL values are less than 15% of the dataset. The 2012 dataset, collected in the Delaware Bay, did not have pha data so values were estimated from the %pha from similar Delaware Bay sites (Gosnell et al., 2015) and make up 20% of the dataset. Below detection limit and estimated values are indicated in the data table (Table S2). The data normality was evaluated using the Shapiro-Wilks test. Most of the variables had a non-normal distribution and were normalized using Box-Cox normalization in Excel with the add-in real statistics resource pack. The Box-Cox lambda values were determined with the add-in package using the boxcoxlambda() function. Outliers were defined as values greater/less than 1.5 times the interquartile range and are referred to as either "elevated" or "low" in the text.

All sites were initially included for the statistical analyses, referred to as the Full Model throughout the text (55 individuals). The data were also evaluated with the contaminated sites removed (those with >400 ng/g sediment HgT), referred to as the Reduced Model (39 individuals). The value of 400 ng/g was chosen as it represents the median value between the Effects Range Levels defined by the NOAA sediment quality guidelines for estuarine sediment (Long et al., 1995). Additionally, the value was between those sites that are known to be historically contaminated by point source inputs and those that are not (Fig. S3). All sites are listed in Table 1 and those that were considered contaminated are marked with an asterisk after the site code. There were not enough sites to run the contaminated sites independent of the uncontaminated sites.

2.4.1. Linear Relationships

Many single estuary studies have found strong and consistent linear relationships between Hg and carbon (OC) variables. Therefore, linear relationships between such variables (p-, d-, and sediment HgT and MeHg, DOC, %LOI) were tested on the log transformed Full and Reduced Datasets. The correlations were plotted in R (version 3.5.0) as an x, y function with a linear model correlation added ($Im(y^x)$). Correlation coefficients (r) were determined with $cor{stats}$ in R (cor(x, y, method="pearson") and p values were determined with $cor.test{stats}$. The linear correlation and correlation statistical results were plotted together using the pairs{graphics} function in R, and symbols were added to the plot to represent various levels of significance (<0.001=***, 0.001-0.01=**, 0.01-0.05=*, 0.05-0.1=:, and <math>>0.1= blank).

General linear relationships between all variables were identified using a Pearson's correlation matrix made with the corrplot library on the boxcox normalized datasets used in the PCA analysis. Only significant relationships are shown in the correlation matrices, with significance defined as p<0.01. The variables were arranged qualitatively by type and are consistent between the Full and Reduced Model for easy comparison.

2.4.2. Principal Component Analysis.

Principal component analyses (PCA) were used to visualize the relationships between all variables in the Full and Reduced datasets. All data included in the PCA were Box-Cox normalized and z-score standardized in Excel. The PCA was completed in R using the prcomp() function from the stats package and included 23 variables (Table S1, all but calculated Hg variables). The variables and individuals (sites) were plotted separately to help with data visualization (Abdi and Williams, 2010). The variables were plotted based on the correlation between each variable and the first and second principal components. Variables that are positively correlated group together, and those that are negatively correlated lie on opposite sides of the plot. Variables that lie further from the plot origin are better represented by the first and second components of the PCA. The PCA individuals (sites) are plotted based on their PC loadings. Individuals that are similar group together on the plot (Abdi and Williams, 2010).

2.4.3. Partial Least Squares Regression Models

Partial least squares regression models (PLSRM) were carried out using the mvr(method=oscorespls; orthogonal scores partial least squares) function within the pls

package in R. The results were cross validated (validation= "LOO") and the output evaluated using functions included in the statistical package including summary(), scores() and loadings(). 21 variables were included in the MeHg PLSRM models. All MeHg variables were excluded from the HgT models since MeHg is a component of HgT (18 variables remained). The number of components used in the PLSRM was determined in R using the selectNcomp() function (Mevik and Wehrens, 2015). The final model had the fewest number of components without being significantly different than the reference model (p=0.01, method=randomization). The results were converted to Variable Influence on Projections (VIP) scores (Chong and Jun, 2005), and since the average of the squared VIP scores equals 1, variables with VIP scores greater than 1 were considered highly influential (Chong and Jun, 2005). R² values were used to indicate how much of the variability in the dependent variables was described by the PLSR models (Wold et al., 2001).

3. Results

3.1. Site Characteristics and Variable Concentration Ranges

The sites included in this survey fall within three unique regions of watershed land-use: forested, developed, and agriculture/wetland (Fig S2). In general, the northern latitude sites have watersheds dominated by forests and shrub land with little urban development except for site A within the Penobscot River. The Berry's Creek watershed in New Jersey is highly developed, as well as the sites along the Delaware River near Philadelphia, PA. The downstream Delaware Bay sites, away from Philadelphia, were characterized by agricultural land cover and wetlands with little urban development. Sites in Connecticut, as well as those from the

Chesapeake Bay in Maryland, fell closest to the center of the PCA diagram (Fig. S2), indicating a more mixed watershed land use signal.

291

292

293

294

295

296

297

298

299

300

301

302

303

304

305

306

307

308

309

310

311

312

The sites sampled also encompassed a large range in Hg and C loading. The range, mean, median and standard deviation of all variables are given in Table S1. The water column and sediment MeHg (dMeHg= 0.002-1.49 ng/L, pMeHg= 0.10-22.58 ng/g, sediment MeHg= 0.01-4.96 ng/g) and HgT (dHgT= 0.20-3.95 ng/L, pHgT= 1.87-721.0 ng/g, sediment HgT= 0.44-287.35 ng/g) concentrations used in the reduced model are similar to those measured in previous estuarine studies along the NE coast of the United States (e.g. Balcom et al., 2015; Heyes et al., 2006; Mason et al., 1999; Gosnell et al., 2015; Schartup et al., 2013) and other temperate regions, including San Francisco Bay (e.g. Conaway et al., 2003), Europe (e.g. Sweden; Jonsson et al., 2014) and Asia (e.g. China; Jiang et al., 2017). For sites without point source Hg contamination, sediment Hg levels are generally <200 ng/g (Table S2). Two sites in the Delaware River had sediment Hg between 200 and 300 ng/g. The concentrations measured at known point-source contaminated areas (dMeHg= 0.013-1.491 ng/L, pMeHg= 1.16-55.31 ng/g, sediment MeHg= 2.01-62.53 ng/g, dHgT= 0.91-11.86 ng/L, pHgT= 85.64-3433.35 ng/g, sediment HgT= 364.75-36034.13 ng/g) also agree with other studies at those sites (e.g. Cardona-marek et al., 2007; Merritt and Amirbahman, 2008; Gilmour et al., 2018; Yeager et al., 2018). The contaminated locations on the Penobscot River had values above 500 ng/g while the locations in the Hackensack River and Berry's Creek ranged in concentrations from 142 to 36034 ng/g (Table S2). Dissolved MeHg concentrations were <0.25 ng/L for all sites except two noncontaminated systems with elevated water column MeHg levels (i.e. Mount Desert Island (NEC-H, NEC-L, BH-H, and BH-L) and Barn Island (BI-H and BI-L)), which is consistent with prior studies (Balcom et al., 2015; Bank et al., 2007; Chen et al., 2014; Langer et al., 2001), and the contaminated sites.

313

314

315

316

317

318

319

320

321

322

323

324

325

326

327

328

329

330

331

332

333

In general, Hg levels at the contaminated sites were elevated in the dataset. Sites within the Berry's Creek System had elevated MeHg and HgT levels in the dissolved, particulate, and sediment phases, except for pMeHg at site 3A (Table S2). The Penobscot River had elevated sediment MeHg concentrations at sites M, O, and V. The only elevated water column variable found within the Penobscot was the suspended pHgT at A, which is a site upstream of a location of historical Hg release (site O). Sites from the northernmost sampled region in Maine, BH-H and -L on Mount Desert Island, had elevated water column p and dMeHg levels. Further, BH-L had elevated DOC and pha concentrations and BH-H had elevated sediment %LOI. BI, in CT, specifically for the 2013 field season, had elevated levels of dMeHg at the HOC site, as well as pMeHg, %MeHg (p- and d-), chl a and pha at both the HOC and LOC subsites. Notably, the noncontaminated sites with elevated Hg levels also had elevated C proxy variables (specifically DOC, %LOI, chl a, and pha), whereas the contaminated sites were strictly elevated in Hg. SB (HOC and LOC) in the Delaware Bay had highly elevated DOC and TSS concentrations, but the sites were not elevated in HgT or MeHg. Other sites within the Delaware Lower Bay (WB and NB) had elevated TSS, which was consistent across sampling years (2012 and 2015).

3.2. Statistical Relationships Among Variables

Correlations used to evaluate relationships between variables are often shown to relate to each other within estuarine systems (HgT, MeHg, DOC, %LOI; Fig. 1 and 2). A select number of HgT and OC variables are plotted in the SI to show differences more clearly between the

contaminated and uncontaminated sites (Fig. S3). Overall, the Full Model (all sites included) had many more significant relationships than the Reduced Model, which excluded sites with sediment >400 ng/g DW to examine controls for uncontaminated locations. These differences were conceivably driven by the outliers at the contaminated sites. In fact, of the 28 relationships explored, 24 relationships were significant (p<0.05) with 17 of those being highly significant (p<0.001). The only variable that did not consistently correlate with the other parameters in the Full dataset was DOC, which only correlated with the dHgT, dMeHg, and pMeHg (Fig. 1). The relationship between DOC and pMeHg likely reflects the strong correlation between dMeHg and pMeHg (r=0.76; p<0.001) rather than a direct relationship between DOC and pMeHg (r=0.38). The Reduced Model correlation matrix resulted in 14 significant relationships (p<0.05), with 7 being p<0.001 (Fig. 2). The only relationships that had higher regression coefficients in the reduced dataset were between DOC and dHgT (r=0.58 in the Full, and r=0.70 in the Reduced) and between %LOI and sediment HgT (r=0.63 in the Full, and r=0.65 in the Reduced). Significant relationships (p<0.01) between all variables are shown in Fig. S5 for both the Full (Fig. S5a) and Reduced (Fig. S5b) Models and details of the correlation matrix are discussed in section 4.1.

334

335

336

337

338

339

340

341

342

343

344

345

346

347

348

349

350

351

352

353

354

355

Principal component analyses were used to assess the more dynamic relationships between the variables (Figs. 3, 4, and S4). In the PCA plots the sites are colored by the system from which they were sampled, listed in Table 1, but note that the Penobscot Sites are grouped in the Reduced model. The groupings do not impact the results of the statistical analysis, only the visual outputs. Overall, the Full PCA Model (Fig. 3, and S4a) resulted in the majority of the data variance being described by positively correlated Hg variables, specifically pHgT and sediment

HgT followed by dHgT, pMeHg, and sediment MeHg along the first component (Dim1= 27.6%). Pha and latitude contributed most to the variance along the second component (Dim2 = 15.2%) and were negatively correlated to each other. The plot of Full Model individuals showed site separation with a lack of a consistent latitudinal or regional trend (Fig 3a). In the Reduced PCA Model (Fig. 4, and S4b), the main variables loading on the first component were pHgT, conductivity and salinity (Dim1= 23.1%), with pHgT negatively correlated to the other two, and the second component was driven by temperature and latitude (Dim2= 18.3%), which were negatively correlated. The individual locations showed system separation similar to the Full Model but with a more latitudinal trend, specifically separating the Chesapeake and Delaware systems from the rest along the second component. In both models, 5 components were needed to capture >75% of the variability in the dataset.

3.3. Partial Least Squares Regression Model Results

Partial Least Squares Regression (PLSR) models were run for MeHg and HgT in their dissolved and particulate phases, for the Full and Reduced Models. The number of components used in each model and the model fit results can be found in Table S3. The interpretation of the PLSRM result focuses on the most influential variables with VIP scores greater than 1 (Chong and Jun, 2005). The Full Model and Reduced Model VIP scores are plotted against each other to graphically display how the results shift when the contaminated sites are removed (Fig. 5 and 6). In each figure, the Full Model results are plotted on the x-axis and the Reduced Model results on the y-axis. A 1:1 line was drawn on the plots; variables that fall on the line have

similar VIP scores in both models. Variables that plot below the 1:1 line projected higher in the Full Model, and those above projected higher in the Reduced Model.

The variables strongly influencing pHgT for the entire dataset included sediment HgT, % forest/shrub land cover, dHgT, chl a, salinity, % low developed land cover, conductivity, and rainfall (Fig. 5a). The Reduced Model differed from the Full Model with the most influential variable being catchment size, which was <1 in the Full Model, followed by conductivity, salinity, chl a, sediment HgT, % forested land cover, and rainfall. The % low developed land cover and dHgT were no longer important in the Reduced Model. The Full Model dHgT variables of importance were sediment HgT, DOC, pHgT, % forested land cover, sediment %LOI, and pha (Fig. 5b). The dHgT Reduced Model had the fewest predicted important variables (three) and was dominated by DOC (VIP>2), followed by % highly developed land use and pHgT. Few variables in both HgT model comparisons fell on the 1:1 line (y= 0.61x+0.31; R²=0.31 and y= 0.53x+0.41; R²=0.27, respectively) indicating that HgT cycling dynamics in contaminated versus non-contaminated sites is more dissimilar than was found for MeHg.

The most influential variables in the pMeHg Full Model included dHgT, dMeHg, and pHgT followed by sediment HgT, chl a, sediment MeHg, DOC, and % forested land cover (Fig. 6a). The Reduced Model results were similar to the full model except the VIP scores for sediment Hg and % forested land cover were below one, and pH and TSS scores exceeded one with similar VIP scores to DOC. The remaining five variables (dMeHg, dHgT, pHgT, chl a, and DOC) had similar VIP scores between the two models. Dissolved MeHg in the Full Model was strongly influenced by several variables as well, most strongly pMeHg and dHgT (VIP>2) followed by sediment %LOI,

DOC, pHgT, sediment HgT, sediment MeHg, catchment size and % agricultural land use (Fig. 6b). The dMeHg Reduced Model results were similar to the Full Model except the VIP scores for the sediment variables (MeHg and HgT), pHgT and catchment size were below one. Similar to pMeHg, pH was an important predictive variable only in the Reduced Model. Many of the dissolved and particulate MeHg variables fell near the 1:1 line, with an overall regression slope near 1 (y= 0.96x-0.02; R²= 0.74 and y=0.93x+0.04; R²= 0.70, respectively) suggesting MeHg cycling is similar between contaminated and uncontaminated sites.

4. Discussion

4.1. General Mercury Characteristics by Site

It is known that Hg concentrations in estuarine waters are impacted by their local watershed and estuarine dynamics, and relationships between Hg concentrations and estuarine parameters have been used to identify Hg sources and mobility in aquatic systems. For instance, strong relationships between inorganic Hg and DOC/ TSS have been used to show the dominance of watershed HgT export to estuaries (Benoit et al., 1998; Grigal, 2002; Laurier et al., 2003; Pato et al., 2010). Relationships have also been observed between estuarine Hg and local land use (Obrist et al., 2018), the tidal stage (Balcom et al., 2015; Pato et al., 2010) and with the degree of Hg contamination (Jiang et al., 2017; Schaefer et al., 2004). MeHg sources to estuaries are generally more complex than HgT (Buckman et al., 2017; Chen et al., 2014; Choe and Gill, 2003). Sediments were once focused on as a dominant source of MeHg to the estuarine water column (Hammerschmidt et al., 2004; Hammerschmidt and Fitzgerald, 2008; Schartup et al., 2013), but more recent work has demonstrated that the link is not

straightforward (Balcom et al., 2015; Seelen et al., 2018; Shi et al., 2018). Rather, MeHg in estuarine waters may be more closely linked to water column production (Schartup et al., 2015a) similar to the open ocean (Blum et al., 2013).

In this study, the sites sampled generally fell within three distinct land use regions that had a latitudinal trend. Less developed watersheds were present in the northern part of the study region and more developed or agricultural watersheds were present in the south. The two sampled contaminated estuaries had unique watershed land-use; the Penobscot is dominantly forested, while the Berry's Creek/ Hackensack watershed is predominantly developed.

However, when analyzed together on a full variable, Full Model PCA plot (Fig. 3), the two contaminated sites fell into the same quadrant with only one other system suggesting the contaminated sites have similar qualities. The region that grouped closest to the contaminated sites were those from Mount Desert Island, Maine, which had elevated water column pMeHg and dMeHg coinciding with elevated DOC and %LOI, which is likely why it grouped with the contaminated sites. The high Hg/OC relationship observed at the contaminated sites, however, suggests that the Hg levels are unnatural and not due to DOC related transport from the watershed (Fig. S3).

The co-export of HgT with organic matter from the watershed indicates that they are generally strongly linked in uncontaminated estuaries (Bergamaschi et al., 2012; Stoken et al., 2016). However, if one variable is altered significantly due to anthropogenic activity, the correlations will fall outside typical regression relationships (Jiang et al., 2017). Indeed, Hg/OC anomalies in sediment cores have been used to infer anthropogenic Hg contamination (e.g. Schartup et al.,

2013). The contaminated sites here had sediment HgT varying by almost 5 orders of magnitude, but the sediment %LOI varied by only a factor of 40 (0.7 – 27%). Further, the HgT/%LOI was elevated relative to uncontaminated sites (Fig. S3) supporting their allocation as contaminated and not driven by OC export. The highly elevated sediment Hg concentrations were reciprocated by the water column, although there was a much smaller range of HgT and MeHg observed with concentrations ranging 3-4 orders of magnitude in the water.

439

440

441

442

443

444

445

446

447

448

449

450

451

452

453

454

455

456

457

458

459

460

Correlation matrix plots between all variables in the Full (Fig. S5a) and Reduced (Fig. S5b) models exemplify the differences between the two datasets, and therefore inferred differences between contaminated and uncontaminated sites, with some interesting trends. Nearly all measured Hg variables correlated with the watershed land use variables in the Full dataset. However, we suggest these correlations are driven by the outliers and are not truly diagnostic of the influence of land use on the coastal Hg cycle. In contrast, at the uncontaminated sites, the relationships with watershed variables are similar to what other studies have found, such as forests slowing the movement of HgT from the watershed (Obrist et al., 2011a; Porvari et al., 2003) and developed land increasing overland pHgT fluxes (Eckley and Branfireun, 2008; Hsu-Kim et al., 2018). It is also noted that the correlations between calculated Hg variables (%MeHg and Kd) and the OC-related variables generally improved in the Reduced dataset compared to the Full Model. Such variables were not included in the multivariate analyses (PCA and PLSRM) to maintain variable independence. Total OC has been suggested as a proxy for net methylation assuming that demethylation is essentially constant (Lambertsson and Nilsson, 2006) which is not true at contaminated sites (Schaefer et al., 2004), supporting the stronger relationships in the Reduced Model. More detailed water column studies suggest that OC composition directly

impacts the %MeHg measured in riverine waters (Bravo et al., 2018), which is likely the case in the systems used for this analysis. Indeed, Schartup et al., (2015b) showed that the composition of DOC in estuarine systems influenced Hg reactivity and bioaccumulation into plankton, processes that could also impact %MeHg.

Overall, contaminated sites were found to have unique properties from uncontaminated sites. However, it is recognized that the inclusion of contaminated sites in a multi-estuary analysis can help drive significant correlations, as was demonstrated in the correlation matrices of the Full and Reduced model (Figs. 1 and 2). Therefore, site selection is important when using correlation as a diagnostic tool, and contaminated sites should be considered independently from uncontaminated sites. While there were some general trends between Hg, OC, and land use variables observed in the correlation data, the relationship between them, especially at uncontaminated sites, is not well resolved by only correlation analysis. The following sections review more closely the correlation and multivariate analysis results that were used to better understand the complicated relationships between the sampled variables.

4.2. Sediment Versus Watershed Inputs of HgT

It is acknowledged that, in general, outliers should be excluded from statistical analyses. Their inclusion in this study was to specifically show how local contamination impacts coastal Hg cycling, and how different the results are when those driving variables are removed. Hg is highly particle reactive so its pollution legacy is largely preserved in coastal sediment, but is subject to continual internal recycling due to sediment resuspension (Pato et al., 2010; Seelen et al., 2018). As such, its effects can remain long after primary sources stop discharging Hg. It is

apparent that sites with elevated sediment HgT concentrations impart a stronger linear relationship between the sediment and water column HgT across the sampled systems (Fig. 1) than when these sites are not included (Fig. 2). In fact, one of the strongest correlations found in the Full Hg and OC correlation matrix was between sediment HgT and pHgT (r = 0.78, p<0.001). There was also a significant correlation between sediment HgT and dHgT (r = 0.72, p<0.001), unlike in the reduced model (r = 0.28, p > 0.05), suggesting an overall elevation of Hg in water columns of contaminated systems. The anthropogenic driven elevation of dHgT at contaminated sites becomes very apparent in contaminated sites when evaluating the dHgT and DOC relationship, which was linear at the uncontaminated sites but exponential at contaminated sites (Fig. S3).

Sediment HgT and pHgT were also significant in the Reduced Model although weaker (r = 0.43, p <0.01). We suggest the strong relationship in the reduced model reflects the capture of watershed derived particles before being transported offshore (Amos et al., 2014; Cossa et al., 1997). The weakened relationship in the Reduced Model therefore suggests that continual inputs from the watershed dominate over resuspended input into uncontaminated systems (Seelen et al. 2018). In support of watershed inputs, the strong correlations between pHgT, watershed, and estuarine mixing variables (e.g. salinity, conductivity) (Fig. S5b) imply a riverine, and therefore watershed, input for pHgT at uncontaminated sites. The stronger correlation between dHgT and DOC in the reduced dataset implies that the watershed, not sediment, is also the most important source delivering dHgT to uncontaminated systems consistent with previous reports (Stoken et al., 2016).

The PCA analyses (Figs. 3, 4, and S4) also support a difference in Hg cycling between contaminated and uncontaminated systems, and specifically that the water column and sediments are more closely linked at contaminated sites. This conclusion is made by comparing the variables that load strongly in the Full and Reduced PCA analyses. Variance in the Full Model PCA was driven by the Hg variables overwhelming all other variables. The Reduced Model variance, however, was driven by a suite of variables along the first and second component with many of the Hg variables loading weakly (Fig. 4). These results suggest HgT at uncontaminated sites are driven by whole system dynamics rather than an obvious dominant source, as observed with the sediment source dominating at the contaminated sites. Therefore, while removal of local sediment may help mitigate Hg contamination at contaminated sites, Hg mitigation at other locations will require a more regional approach and consideration of the control of Hg inputs from the watershed. Overall, the need for five components to describe >75% of the data variability in the PCA analysis implies that the sites are too dissimilar to be explained satisfactorily using a principal component analysis for both the Full and Reduced models.

4.3. Sediment Versus Watershed Inputs of MeHg

503

504

505

506

507

508

509

510

511

512

513

514

515

516

517

518

519

520

521

522

523

Sediments have been focused on as a probable primary site for MeHg formation and release into coastal water columns due to their high methylation potential (Hammerschmidt and Fitzgerald, 2004). However, sediment-water exchange fluxes do not always reflect the underlying high sediment methylation rates (Monperrus et al., 2007; Seelen et al., 2018; Shi et al., 2018). Many studies have suggested that alternative sources of MeHg to the water column

may be more important than sediment seasonally (Gosnell et al., 2015; Monperrus et al., 2007), spatially (Buckman et al., 2017; Schartup et al., 2015a), and in terms of Hg bioavailability (Jonsson et al., 2017). Therefore, identifying where MeHg is being produced will help to better understand pathways of exposure. The data collected for this study did not specifically measure net MeHg formation or evaluate in greater detail the OC composition which has been shown to account for MeHg variability in sediment and aquatic environments (Bravo et al., 2017). Therefore, this section focuses on relationships between variables that can be used to infer the importance of sediment vs non-sediment MeHg sources to estuarine water columns. First, it is apparent that MeHg concentrations are more strongly correlated to the sediment and HgT variables in the Full Model (Fig. 1) than the Reduced (Fig. 2). In fact, the decoupling of the sediment-water column signal for Hg species from the Full to Reduced Model was most apparent for MeHg with a strong correlation between sediment MeHg and pMeHg in the Full Model (p<0.001), but no relationship in the Reduced. The sediment- water column relationship in the Full Model implies connectivity between those two pools in contaminated locations, although it is difficult to infer whether the measured water column MeHg was methylated in the sediment or the water column using correlation alone. In the Reduced Dataset (Fig. 2), the observed water column MeHg concentrations more strongly correlated with water column and watershed parameters (p<0.01) such as d- and pHgT, DOC/TSS, pH, and %Agricultural land use. The lack of relationship with the sediment does not necessarily imply that sediment does not contribute to observed water column MeHg concentrations, but, with the evaluation methods used here, the signal is weak or indirect.

524

525

526

527

528

529

530

531

532

533

534

535

536

537

538

539

540

541

542

543

MeHg concentrations are undoubtably related to HgT, with both dMeHg and pMeHg strongly correlated to dHgT in the Reduced dataset (r>0.6, p<0.001). However, the weakened relationships between HgT and MeHg in the Reduced Model suggests a nuanced link between these variables in typical estuarine systems. The lack of correlation between MeHg and parameters predicted to be coupled to HgT, for instance the weak correlation between dMeHg and DOC (r= 0.39, p<0.05) and between pMeHg and salinity, chl a, and sediments (p>0.05) suggest HgT and MeHg have different source/sink dynamics. The weak relationship of MeHg to DOC and sediments, which HgT are correlated to, further suggests that Hg methylation may be occurring in situ. Without more information on Hg sources and methylation potential in coastal waters, it is difficult to conclude with certainty where MeHg is formed. However, the data at hand suggest that HgT leaching from watersheds combined with DOC drive in situ methylation, which is likely a more dominant source of MeHg to water columns than sediment in typical northeast US estuaries. The current analysis offers only weak support for bulk sediment as an important source of MeHg to estuarine water columns, and further demonstrates that there are distinctly different MeHg sources for locally contaminated sites compared to those receiving a regional Hg input signal.

4.4. Predictors for Water Column Mercury

545

546

547

548

549

550

551

552

553

554

555

556

557

558

559

560

561

562

563

564

565

Being able to reduce a large set of ecosystem variables down to a few that best relate to Hg and MeHg concentrations in coastal waters can greatly help researchers in their effort to predict, monitor, model, and manage Hg movement through coastal ecosystems. This study utilized PLSRM to better understand the complex interactions between ecosystem variables and

HgT/MeHg. Our efforts suggest that dHgT is the most predictable Hg fraction due to its tight complexation with DOC. PHgT is the least predictable with many variables correlating to it and influencing its concentration. Both MeHg fractions are strongly linked to HgT and each other, and are the most similar between the Full and Reduced Models suggesting similar source dynamics. HgT and MeHg variable dynamics differ, but all HgT and MeHg concentrations are influenced by historic contamination when it is present. This next section discusses further the PLSRM results supporting these assessments.

566

567

568

569

570

571

572

573

574

575

576

577

578

579

580

581

582

583

584

585

586

587

To reiterate, predictive, or highly correlative variables, were reduced from the full dataset using PLSRM. PLSRMs generate predictive variables for a specific dependent variable. The proxy used to determine which variables are important to predict the concentration of the Hg variables was VIP scores. Variables with VIP scores greater than one were considered strongly predictive and were focused on in this discussion. The PLSRM results were evaluated as a comparison between the Full and Reduced model. In theory, if Hg behaved the similarly in the full and reduced model the VIP scores would remain the same between model runs (variables would fall on the 1:1 line in Figs. 5 and 6). For MeHg, this was predominantly the case, but was not so for HgT. Overall, the VIP scores for HgT were quite different between the Full and Reduced Models in the particulate (Fig. 5a) and dissolved (Fig. 5b) phase suggesting that HgT cycling differs between contaminated and uncontaminated sites. The dHgT was overwhelmingly predicted by DOC in the Reduced Model, which is consistent with previous research suggesting mobilization of dHgT from the watershed by DOC (Grigal, 2002; Hsu-Kim et al., 2018; Taylor et al., 2019). In the Full dHgT Model, sediment HgT and DOC had similar VIP scores implying that legacy Hg impacts dHgT at contaminated locations, but these locations may also have important

watershed inputs. Particulate HgT and dHgT are strongly predictive of each other in their respective Full Models, indicating that partitioning is predictable at contaminated sites similar to the findings of Schartup et al., (2013). However, partitioning does not appear to be consistent across the uncontaminated sites suggesting that dHgT and pHgT have different source dynamics, with slow or kinetically hindered exchange between phases in typical estuarine environments.

Overall, pHgT had the largest number of significantly predictive variables in the PLSR models and the largest shifts between the Full and Reduced Models (Fig. 5a). It was consistently predicted by proxies for estuarine mixing (salinity and conductivity), similar to the PCA results, as well as a proxy for biomass (chl a). The influence of sediment HgT was apparent in both models but to a greater degree in the Full Model. This reiterates the idea that sediment acts as a dominant pHgT source in contaminated sites overwhelming watershed inputs (Balcom et al., 2015), but acts as a dominant sink in the Reduced model with watershed inputs overwhelming inputs from resuspension. The second scenario is likely to be true in most estuarine systems (Seelen et al., 2018), but not necessarily in areas of high bank erosion (Lawson et al., 2001) or turbidity (Balcom et al., 2015; Gosnell et al., 2015). The results of the HgT PLSRM suggest that pHgT is stochastic, influenced by the watershed, and linked to coastal sediment. However, dHgT is more predictable and strongly linked to DOC, except when sites are contaminated where sediment input becomes an important source.

The water column pMeHg and dMeHg PLSRM results suggest that few variables are required to predict their concentrations, which remained similar in both the Full and Reduced Models (Fig.

6). This finding suggests that MeHg net production/cycling are similarly controlled between contaminated and uncontaminated sites. The MeHg forms were strongly linked to each other and to dHgT, as well as metrics for the organic material concentration (chl a, DOC, and %LOI). This finding supports the notion that dHgT is the precursor to MeHg, but the relationship depends on OC (Benoit et al., 2003), and that MeHg partitions predictably once formed. The only watershed land use variable with a VIP score greater than one for either MeHg form was %Agriculture for dMeHg. The link between MeHg and agricultural land use has been noted previously (Lawson et al., 2001; Shanley et al., 2005), but the significance is unclear and may be linked to nutrient inputs (Bonzongo et al., 2016). Sediment levels were only strongly predictive of water column MeHg in the Full Model, and sediment variables were consistently more strongly predictive for HgT than MeHg. The strong relationship with in situ variables, and lack of relationship to the watershed and sediment supports the premise that MeHg is dominantly formed in situ in the spring-summer when the samples were collected. Overall, the PLSRM results suggest that dMeHg and pMeHg have similar controls at contaminated and uncontaminated sites, except with the emergence of a stronger connectivity with the sediment in the Full model. These results suggest that remediation efforts should focus on sediment HgT. In uncontaminated locations, general reduction in Hg emissions and, as a result, watershed fluxes of Hg, would be beneficial. While this study has provided increased understanding for the region and the summer season, further evaluation is needed to extend the relationships to other seasons and locations. However, it is clear that future work should take care to differentiate contaminated from uncontaminated locations and to examine the primary relationships for each independently. Furthermore, we show that a more nuanced examination

609

610

611

612

613

614

615

616

617

618

619

620

621

622

623

624

625

626

627

628

629

can be elucidated from multi-variate analyses across a number of ecosystems than can be acquired from regression analysis alone.

5. Conclusion

631

632

633

634

635

636

637

638

639

640

641

642

643

644

645

646

647

648

649

650

651

The goal of this research was to better understand how Hg cycles through coastal environments, and especially what drives observed water column MeHg levels in temperate estuarine water columns. We found that coastal water column Hg concentrations are strongly impacted by historic contamination of Hg retained in coastal sediments, and the elevated HgT concentrations result in elevated MeHg levels. Sediments, therefore, are an important source of estuarine water column HgT and MeHg in the dissolved and particulate phase at contaminate sites. However, Hg sources differed in uncontaminated systems. Dissolved HgT co-export with DOC from the watershed controlled dHgT concentrations in the uncontaminated estuaries studied. Particulate HgT was more closely linked to physical estuarine properties (salinity and conductivity) and watershed variables (%forested land use, catchment size, and rainfall). This suggests that pHgT is dominantly sourced from the watershed in uncontaminated sites and is removed from the water column via sedimentation. Water column MeHg was more strongly linked to internal rather than external sources, including sediment production and flux. This conclusion is based on the weak predictiveness of sediments on the MeHg concentrations in all PLSRMs, strong MeHg partitioning observed in the water column, and the relationship between MeHg and dHgT and DOC. The similarities between the Full and Reduced models for both pand dMeHg further suggests that their concentrations are similarly controlled in contaminated in uncontaminated sites. Overall, it is concluded that historically contaminated sites should be

considered unique from uncontaminated locations, and sediment should be focused on for remediation or mitigation where significant point source contamination persists. For regionally impacted watersheds, mitigation will need an understanding of the importance of watershed inputs, and not just rely on examination of the local sediment concentrations.

Acknowledgements:

We wish to acknowledge the help of current and past members of the Mason Lab, especially Brian DiMento, Kati Gosnell, Bridget Holohan, Sofi Jonsson, Nash Mazrui, Veronica Tanguay (ne Ortiz), for mercury and ancillary parameter analyses, and help in the field. We also thank the anonymous reviewers for their helpful critiques. This work was supported by grants from the National Institute of Environmental Health Sciences of the National Institute of Health under award P42 ES007373 (NIEHS RO1ES021950), the National Science Foundation Graduate Research Fellowship Grant # DGE-1747453, and the NSF grant to Mason (# OCE-1634048), and the University of Connecticut Marine Science Pre-Doctoral Fellowship Program. The contents of this manuscript are solely the responsibility of the authors and do not necessarily represent official views of NIEHS or NIH.

References

Abdi, H., Williams, L.J., 2010. Principal component analysis. John Wiley Sons, Inc. WIREs Comp Stat 2, 433–459. https://doi.org/10.1002/wics.101

Amos, H.M., Jacob, D.J., Kocman, D., Horowitz, H.M., Zhang, Y., Dutkiewicz, S., Horvat, M., 672 673 Corbitt, E.S., Krabbenhoft, D.P., Sunderland, E.M., 2014. Global biogeochemical implications of mercury discharges from rivers and sediment burial. Environ. Sci. Technol. 674 48, 9514-9522. https://doi.org/10.1021/es502134t 675 Balcom, P.H., Schartup, A.T., Mason, R.P., Chen, C.Y., 2015. Sources of water column 676 677 methylmercury across multiple estuaries in the Northeast U.S. Mar. Chem. 177, 721–730. https://doi.org/10.1016/J.MARCHEM.2015.10.012 678 679 Bank, M.S., Burgess, J.R., Evers, D.C., Loftin, C.S., 2007. Mercury contamination of biota from 680 Acadia National Park, Maine: A review. Environ. Monit. Assess. 126, 105–115. https://doi.org/10.1007/s10661-006-9324-4 681 682 Benoit, J., Gilmour, C., Heyes, A., Mason, R., Miller, C., 2003. Geochemical and biological 683 controls over methylmercury production and degradation in aquatic ecosystems, in: Biogeochemistry of Environmentally Important Trace Elements. pp. 262–297. 684 https://doi.org/10.1021/bk-2003-0835.ch019 685 686 Benoit, J.M., Gilmour, C.C., Mason, R.P., Riedel, G.S., 1998. Behavior of Mercury in the Patuxent River Estuary. Biogeochem. 40 249-265. https://doi.org/10.1023/a:1005905700864 687 Bergamaschi, B. a, Krabbenhoft, D.P., Aiken, G.R., Patino, E., Rumbold, D.G., Orem, W.H., 2012. 688 689 Tidally driven export of dissolved organic carbon, total mercury, and methylmercury from 690 a mangrove-dominated estuary. Environ. Sci. Technol. 46, 1371–8. https://doi.org/10.1021/es2029137 691

Bloom, N.S., Gill, G.A., Cappellino, S., Dobbs, C., McShea, L., Driscoll, C., Mason, R., Rudd, J., 692 693 1999. Speciation and cycling of mercury in Lavaca Bay, Texas, sediments. Environ. Sci. Technol. 33, 7–13. https://doi.org/10.1021/es980379d 694 695 Blum, J.D., Popp, B.N., Drazen, J.C., Choy, C.A., Johnson, M.W., 2013. Methylmercury production below the mixed layer in the North Pacific Ocean. Nat. Geosci. 6, 1–5. 696 697 https://doi.org/10.1038/ngeo1918 698 Bonzongo, J.C.J., Donkor, A.K., Attibayeba, A., Gao, J., 2016. Linking landscape development 699 intensity within watersheds to methyl-mercury accumulation in river sediments. Ambio 45, 196–204. https://doi.org/10.1007/s13280-015-0695-z 700 701 Bravo, A.G., Bouchet, S., Tolu, J., Björn, E., Mateos-Rivera, A., Bertilsson, S., 2017. Molecular 702 composition of organic matter controls methylmercury formation in boreal lakes. Nat. 703 Commun. 8, 1–9. https://doi.org/10.1038/ncomms14255 704 Bravo, A.G., Kothawala, D.N., Attermeyer, K., Tessier, E., Bodmer, P., Ledesma, J.L.J., Audet, J., Casas-Ruiz, J.P., Catalán, N., Cauvy-Fraunié, S., Colls, M., Deininger, A., Evtimova, V. V., 705 706 Fonvielle, J.A., Fuß, T., Gilbert, P., Herrero Ortega, S., Liu, L., Mendoza-Lera, C., Monteiro, J., Mor, J.-R., Nagler, M., Niedrist, G.H., Nydahl, A.C., Pastor, A., Pegg, J., Gutmann Roberts, 707 708 C., Pilotto, F., Portela, A.P., González-Quijano, C.R., Romero, F., Rulík, M., Amouroux, D., 709 2018. The interplay between total mercury, methylmercury and dissolved organic matter 710 in fluvial systems: A latitudinal study across Europe. Water Res. 144, 172–182.

https://doi.org/10.1016/J.WATRES.2018.06.064

- Buckman, K., Taylor, V., Broadley, H., Hocking, D., Balcom, P., Mason, R., Nislow, K., Chen, C.,
- 713 2017. Methylmercury Bioaccumulation in an Urban Estuary: Delaware River, USA. Estuaries
- 714 and Coasts 40, 1358–1370. https://doi.org/10.1007/s12237-017-0232-3
- 715 Cardona-marek, T., Schaefer, J., Ellickson, K., Barkay, T., Reinfelder, J.R., 2007. Mercury
- speciation, reactivity, and bioavailability in a highly contaminated estuary Berry's Creek,
- 717 New Jersey Meadowlands. Environ. Sci. Technol. 41, 8268–8274.
- 718 Chen, C.Y., Borsuk, M.E., Bugge, D.M., Hollweg, T., Balcom, P.H., Ward, D.M., Williams, J.,
- Mason, R.P., 2014. Benthic and pelagic pathways of methylmercury bioaccumulation in
- estuarine food webs of the Northeast United States. PLoS One 9.
- 721 https://doi.org/10.1371/journal.pone.0089305
- 722 Choe, K.-Y.Y., Gill, G.A., 2003. Distribution of particulate, colloidal, and dissolved mercury in San
- 723 Francisco Bay estuary. 2. Monomethyl mercury. Limnol. Oceanogr. 48, 1547–1556.
- 724 https://doi.org/10.4319/lo.2003.48.4.1547
- 725 Chong, I.G., Jun, C.H., 2005. Performance of some variable selection methods when
- 726 multicollinearity is present. Chemom. Intell. Lab. Syst. 78, 103–112.
- 727 https://doi.org/10.1016/j.chemolab.2004.12.011
- 728 Conaway, C.H., Squire, S., Mason, R.P., Flegal, A.R., 2003. Mercury speciation in the San
- 729 Francisco Bay estuary. Mar. Chem. 80, 199–225. https://doi.org/10.1016/S0304-
- 730 4203(02)00135-4
- 731 Cossa, D., Martin, J.M., Takayanagi, K., Sanjuan, J., 1997. The distribution and cycling of mercury

- species in the western Mediterranean. Deep. Res. Part II Top. Stud. Oceanogr. 44, 721–
- 733 740. https://doi.org/10.1016/S0967-0645(96)00097-5
- Dean, W.E. jr., 1974. Determination of carbonate and organic matter in calcareous sediments
- and sedmentary rocks by loss on ignition: Comparison with other methods. J. Sediment.
- 736 Petrol. 44, 242–248. https://doi.org/10.1128/JCM.01030-15
- 737 Descriptions of PRISM Spatial Climate Datasets for the Conterminous United States, 2019. ,
- 738 http://www.prism.oregonstate.edu/documents/PRISM_datasets.pdf.
- 739 Driscoll, C.T., Hammerschmidt, C.R., Gilmour, C.C., Greenfield, B.K., Buckman, K.L., Lamborg,
- 740 C.H., Chen, C.Y., Hammerschmidt, C.R., Mason, R.P., Gilmour, C.C., Sunderland, E.M.,
- Greenfield, B.K., Buckman, K.L., Lamborg, C.H., 2012. Nutrient supply and mercury
- 742 dynamics in marine ecosystems: a conceptual model. Environ. Res. 119, 118–31.
- 743 https://doi.org/10.1016/j.envres.2012.05.002
- 744 Eckley, C.S., Branfireun, B., 2008. Mercury mobilization in urban stormwater runoff. Sci. Total
- 745 Environ. 403, 164–177. https://doi.org/10.1016/j.scitotenv.2008.05.021
- 746 EPA, 2000. Guidance for Data Quality Assessment Practical Methods for Data Analysis. U.S.
- 747 Environ. Prot. Agency 219.
- Gilmour, C., Bell, J.T., Soren, A.B., Riedel, Georgia, Riedel, Gerhardt, Kopec, A.D., Bodaly, R.A.,
- 749 2018. Distribution and biogeochemical controls on net methylmercury production in
- 750 Penobscot River marshes and sediment. Sci. Total Environ. 640–641, 555–569.
- 751 https://doi.org/10.1016/j.scitotenv.2018.05.276

Gosnell, K., Balcom, P., Ortiz, V., Dimento, B., Schartup, A.T., Greene, R., 2015. Seasonal Cycling 752 753 and Transport of Mercury and Methylmercury in the Turbidity Maximum of the Delaware Estuary. Aquat. Geochemistry 22, 313–336. https://doi.org/10.1007/s10498-015-9283-x 754 755 Grigal, D.F., 2002. Inputs and outputs of mercury from terrestrial watersheds: A review. Environ. Rev. 10, 1–39. https://doi.org/10.1139/a01-013 756 Hammerschmidt, C.R., Fitzgerald, W.F., 2008. Sediment-water exchange of methylmercury 757 758 determined from shipboard benthic flux chambers. Mar. Chem. 109, 86–97. 759 https://doi.org/10.1016/j.marchem.2007.12.006 Hammerschmidt, C.R., Fitzgerald, W.F., 2006. Bioaccumulation and trophic transfer of 760 761 methylmercury in Long Island Sound. Arch. Environ. Contam. Toxicol. 51, 416–24. 762 https://doi.org/10.1007/s00244-005-0265-7 763 Hammerschmidt, C.R., Fitzgerald, W.F., 2004. Geochemical controls on the production and 764 distribution of methylmercury in near-shore marine sediments. Environ. Sci. Technol. 38, 1487–95. https://doi.org/10.1021/es034528q 765 Hammerschmidt, C.R., Fitzgerald, W.F., 2001. Formation of artifact methylmercury during 766 extraction from a sediment reference material. Anal. Chem. 73, 5930-5936. 767 https://doi.org/10.1021/ac010721w 768 769 Hammerschmidt, C.R., Fitzgerald, W.F., Lamborg, C.H., Balcom, P.H., Visscher, P.T., 2004. 770 Biogeochemistry of methylmercury in sediments of Long Island Sound. Mar. Chem. 90, 31-

52. https://doi.org/10.1016/j.marchem.2004.02.024

- Heyes, A., Mason, R.P., Kim, E.-H., Sunderland, E., 2006. Mercury methylation in estuaries:
- 773 Insights from using measuring rates using stable mercury isotopes. Mar. Chem. 102, 134–
- 774 147. https://doi.org/10.1016/j.marchem.2005.09.018
- 775 Hsu-Kim, H., Eckley, C.S., Achá, D., Feng, X., Gilmour, C.C., Jonsson, S., Mitchell, C.P.J., 2018.
- 776 Challenges and opportunities for managing aquatic mercury pollution in altered
- 777 landscapes. Ambio 47, 141–169. https://doi.org/10.1007/s13280-017-1006-7
- Jiang, T., Skyllberg, U., Björn, E., Green, N.W., Tang, J., Wang, D., Gao, J., Li, C., 2017.
- 779 Characteristics of dissolved organic matter (DOM) and relationship with dissolved mercury
- in Xiaoqing River-Laizhou Bay estuary, Bohai Sea, China. Environ. Pollut. 223, 19–30.
- 781 https://doi.org/10.1016/j.envpol.2016.12.006
- Jonsson, S., Andersson, A., Nilsson, M.B., Skyllberg, U., Lundberg, E., Schaefer, J.K., Åkerblom,
- 783 S., Björn, E., 2017. Terrestrial discharges mediate trophic shifts and enhance
- methylmercury accumulation in estuarine biota. Sci. Adv. 3, 1–10.
- 785 https://doi.org/10.1126/sciadv.1601239
- Jonsson, S., Skyllberg, U., Nilsson, M.B., Lundberg, E., Andersson, A., Björn, E., 2014.
- Differentiated availability of geochemical mercury pools controls methylmercury levels in
- estuarine sediment and biota. Nat. Commun. 5:4624, DOI: 10.1038.
- 789 https://doi.org/10.1038/ncomms5624
- 790 Kocman, D., Horvat, M., Pirrone, N., Cinnirella, S., 2013. Contribution of contaminated sites to
- 791 the global mercury budget. Environ. Res. 125, 160–170.

- https://doi.org/10.1016/j.envres.2012.12.011
- Lambertsson, L., Nilsson, M., 2006. Organic material: The primary control on mercury
- methylation and ambient methyl mercury concentrations in estuarine sediments. Environ.
- 795 Sci. Technol. 40, 1822–1829. https://doi.org/10.1021/es051785h
- Langer, C.S., Fitzgerald, W.F., Visscher, P.T., Vandal, G.M., 2001. Biogeochemical cycling of
- methylmercury at Barn Island Salt Marsh, Stonington, CT, USA 0, 295–310.
- Laurier, F.J.G., Cossa, D., Gonzalez, J.L., Breviere, E., Sarazin, G., 2003. Mercury transformations
- and exchanges in a high turbidity estuary: The role of organic matter and amorphous
- 800 oxyhydroxides. Geochim. Cosmochim. Acta 67, 3329–3345.
- 801 https://doi.org/10.1016/S0016-7037(03)00081-4
- Lawson, N.M., Mason, R.P., Laporte, J.-M., 2001. The fate and transport of mercury,
- methylmercury, and other trace metals in chesapeake bay tributaries. Water Res. 35, 501–
- 804 515. https://doi.org/10.1016/S0043-1354(00)00267-0
- Lexmond, T.M., De Haan, F.A.M., Frissel, M.J., 1976. On methylation of inorganic mercury and
- the decomposition of organo-mercury compounds-a review. Netherlands J.Agric.Sci. 24,
- 807 79–97.

- 808 Long, E.R., Macdonald, D.D., Smith, S.L., Calder, F.D., 1995. Incidence of adverse biological
- 809 effects within ranges of chemical concentrations in marine and estuarine sediments.
- 810 Environ. Manage. 19, 81–97. https://doi.org/10.1007/BF02472006

Lyman, S.N., Jaffe, D.A., 2012. Formation and fate of oxidized mercury in the upper troposphere 811 812 and lower stratosphere. Nat. Geosci. 5, 114–117. https://doi.org/10.1038/ngeo1353 Mason, R., Lawson, N., Lawrence, A., 1999. Mercury in the Chesapeake Bay. Mar. Chem. 65, 77-813 96. 814 Mason, R.P., Choi, A.L., Fitzgerald, W.F., Hammerschmidt, C.R., Lamborg, C.H., Soerensen, A.L., 815 Sunderland, E.M., 2012. Mercury biogeochemical cycling in the ocean and policy 816 817 implications. Environ. Res. 119, 101–117. https://doi.org/10.1016/j.envres.2012.03.013 Merritt, K. a., Amirbahman, A., 2008. Methylmercury cycling in estuarine sediment pore waters 818 (Penobscot River estuary, Maine, USA). Limnol. Oceanogr. 53, 1064–1075. 819 https://doi.org/10.4319/lo.2008.53.3.1064 820 Mevik, B., Wehrens, R., 2015. Introduction to the pls Package. Help Sect. "pls" Packag. RStudio 821 822 Softw. 1-23. 823 Mitchell, C.P.J., Jordan, T.E., Heyes, A., Gilmour, C.C., 2012. Tidal exchange of total mercury and 824 methylmercury between a salt marsh and a Chesapeake Bay sub-estuary. Biogeochemistry 111, 583-600. https://doi.org/10.1007/s10533-011-9691-y 825 Monperrus, M., Tessier, E., Amouroux, D., Leynaert, A., Huonnic, P., Donard, O.F.X., 2007. 826 827 Mercury methylation, demethylation and reduction rates in coastal and marine surface 828 waters of the Mediterranean Sea. Mar. Chem. 107, 49-63. 829 https://doi.org/10.1016/j.marchem.2007.01.018

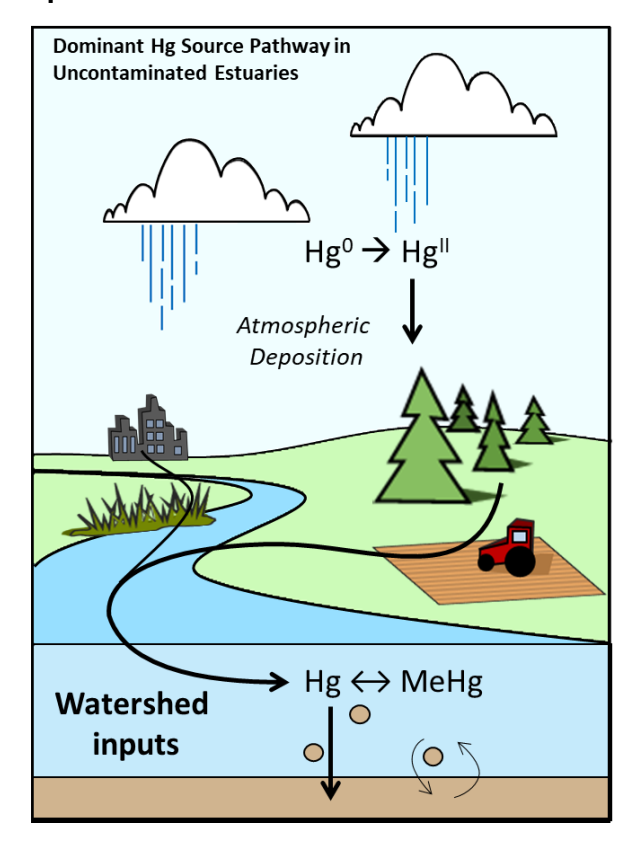
Munson, K.M., Babi, D., Lamborg, C.H., 2014. Determination of monomethylmercury from 830 831 seawater with ascorbic acid-assisted direct ethylation. Limnol. Oceanogr. Methods 12, 1–9. https://doi.org/10.4319/lom.2014.12.1 832 833 Obrist, D., Johnson, D.W., Lindberg, S.E., Luo, Y., Hararuk, O., Bracho, R., Battles, J.J., Dail, D.B., Edmonds, R.L., Monson, R.K., Ollinger, S. V., Pallardy, S.G., Pregitzer, K.S., Todd, D.E., 834 835 2011a. Mercury distribution across 14 U.S. Forests. Part I: Spatial patterns of concentrations in biomass, litter, and soils. Environ. Sci. Technol. 45, 3974-3981. 836 837 https://doi.org/10.1021/es104384m Obrist, D., Kirk, J.L., Zhang, L., Sunderland, E.M., Jiskra, M., Selin, N.E., 2018. A review of global 838 839 environmental mercury processes in response to human and natural perturbations: Changes of emissions, climate, and land use. Ambio 47, 116–140. 840 https://doi.org/10.1007/s13280-017-1004-9 841 Obrist, D., Tas, E., Peleg, M., Matveev, V., Faïn, X., Asaf, D., Luria, M., 2011b. Bromine-induced 842 oxidation of mercury in the mid-latitude atmosphere. Nat. Geosci. 4, 22–26. 843 https://doi.org/10.1038/ngeo1018 844 Outridge, P.M., Mason, R.P., Wang, F., Guerrero, S., Heimbürger-Boavida, L.E., 2018. Updated 845 Global and Oceanic Mercury Budgets for the United Nations Global Mercury Assessment 846 847 2018. Environ. Sci. Technol. 52, 11466–11477. https://doi.org/10.1021/acs.est.8b01246 848 Pato, P., Otero, M., Válega, M., Lopes, C.B., Pereira, M.E., Duarte, A.C., 2010. Mercury partition in the interface between a contaminated lagoon and the ocean: the role of particulate load 849

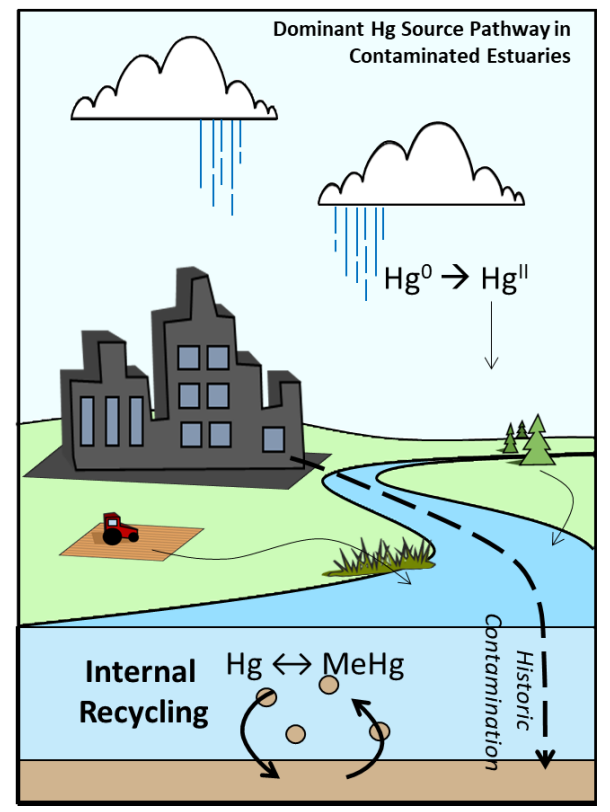
850	and composition. Mar. Pollut. Bull. 60, 1658–66.
851	https://doi.org/10.1016/j.marpolbul.2010.07.004
852	Porvari, P., Verta, M., Munthe, J., Haapanen, M., 2003. Forestry practices increase mercury and
853	methyl mercury output from boreal forest catchments. Environ. Sci. Technol. 37, 2389-
854	2393. https://doi.org/10.1021/es0340174
855	Schaefer, J.K., Yagi, J., Reinfelder, J.R., Cardona, T., Ellickson, K.M., Tel-Or, S., Barkay, T., 2004.
856	Role of the bacterial organomercury lyase (MerB) in controlling methylmercury
857	accumulation in mercury-contaminated natural waters. Environ. Sci. Technol. 38, 4304-
858	4311. https://doi.org/10.1021/es049895w
859	Schartup, A.T., Balcom, P.H., Soerensen, A.L., Gosnell, K.J., Calder, R.S.D., 2015a. Freshwater
860	discharges drive high levels of methylmercury in Arctic marine biota. PNAS 112, 11789-
861	11794. https://doi.org/10.1073/pnas.1505541112
862	Schartup, A.T., Mason, R.P., Balcom, P.H., Hollweg, T.A., Chen, C.Y., 2013. Methylmercury
863	production in estuarine sediments: Role of organic matter. Environ. Sci. Technol. 47, 695–
864	700. https://doi.org/10.1021/es302566w
865	Schartup, A.T., Ndu, U., Balcom, P.H., Mason, R.P., Sunderland, E.M., 2015b. Contrasting effects
866	of marine and terrestrially derived dissolved organic matter on mercury speciation and
867	bioavailability in seawater. Environ. Sci. Technol. 49, 5965–5972.
868	https://doi.org/10.1021/es506274x
869	Seelen, E.A., Massey, G.M., Mason, R.P., 2018. Role of Sediment Resuspension on Estuarine

870	Suspended Particulate Mercury Dynamics. Environ. Sci. Technol. 52, 7736–7744.
871	https://doi.org/10.1021/acs.est.8b01920
872	Selin, N.E., Sunderland, E.M., Knightes, C.D., Mason, R.P., 2010. Sources of mercury exposure
873	for U.S. seafood consumers: Implications for policy. Environ. Health Perspect. 118, 137–
874	143. https://doi.org/10.1289/ehp.0900811
875	Shanley, J.B., Kamman, N.C., Clair, T.A., Chalmers, A., 2005. Physical controls on total and
876	methylmercury concentrations in streams and lakes of the northeastern USA.
877	Ecotoxicology 14, 125–134. https://doi.org/10.1007/s10646-004-6264-z
878	Shi, X., Mason, R.P., Charette, M.A., Mazrui, N.M., Cai, P., 2018. Mercury flux from salt marsh
879	sediments: Insights from a comparison between 224 Ra/228 Th disequilibrium and core
880	incubation methods. Geochim. Cosmochim. Acta 222, 569–583.
881	https://doi.org/10.1016/j.gca.2017.10.033
882	Stoken, O.M., Riscassi, A.L., Scanlon, T.M., 2016. Association of dissolved mercury with
883	dissolved organic carbon in U.S. rivers and streams: The role of watershed soil organic
884	carbon. Water Resour. Res. 52, 3040–3051. https://doi.org/10.1111/j.1752-
885	1688.1969.tb04897.x
886	Sunderland, E.M., 2007. Mercury exposure from domestic and imported estuarine and marine
887	fish in the U.S. seafood market. Environ. Health Perspect. 115, 235–242.
888	https://doi.org/10.1289/ehp.9377
889	Taylor, V., Buckman, K., Seelen, E., Mazrui, N., Balcom, P., Mason, R., Chen, C., 2018. Organic

890	carbon content drives methylmercury levels in the water column and in estuarine food
891	webs across latitudes in the Northeast United States. Environ. Pollut. 246, 639–649.
892	https://doi.org/10.1016/j.envpol.2018.12.064
893	Taylor, V.F., Buckman, K.L., Seelen, E.A., Balcom, P.H., Mazrui, N.M., Mason, R.P., Chen, C.Y.,
894	2019. Organic carbon content drives methylmercury levels in the water column and in
895	estuarine food webs across latitudes in the Northeast United States. Environ. Pollut. 246,
896	639–649.
897	Turner, R.R., Mitchell, C.P.J., Kopec, A.D., Bodaly, R.A., 2018. Tidal fluxes of mercury and
898	methylmercury for Mendall Marsh, Penobscot River estuary, Maine. Sci. Total Environ.
899	637-638, 145-154. https://doi.org/10.1016/j.scitotenv.2018.04.395
900	Wold, S., Sjostrom, M., Eriksson, L., 2001. PLS-regression: a basic tool of chemometrics.
901	Chemom. Intell. Lab. Syst. 58, 109–130. https://doi.org/10.1016/S0169-7439(01)00155-1
902	Yeager, K.M., Schwehr, K.A., Louchouarn, P., Feagin, R.A., Schindler, K.J., Santschi, P.H., 2018.
903	Mercury inputs and redistribution in the Penobscot River and estuary, Maine. Sci. Total
904	Environ. 622–623, 172–183. https://doi.org/10.1016/j.scitotenv.2017.11.334
905	
906	

Graphical Abstract





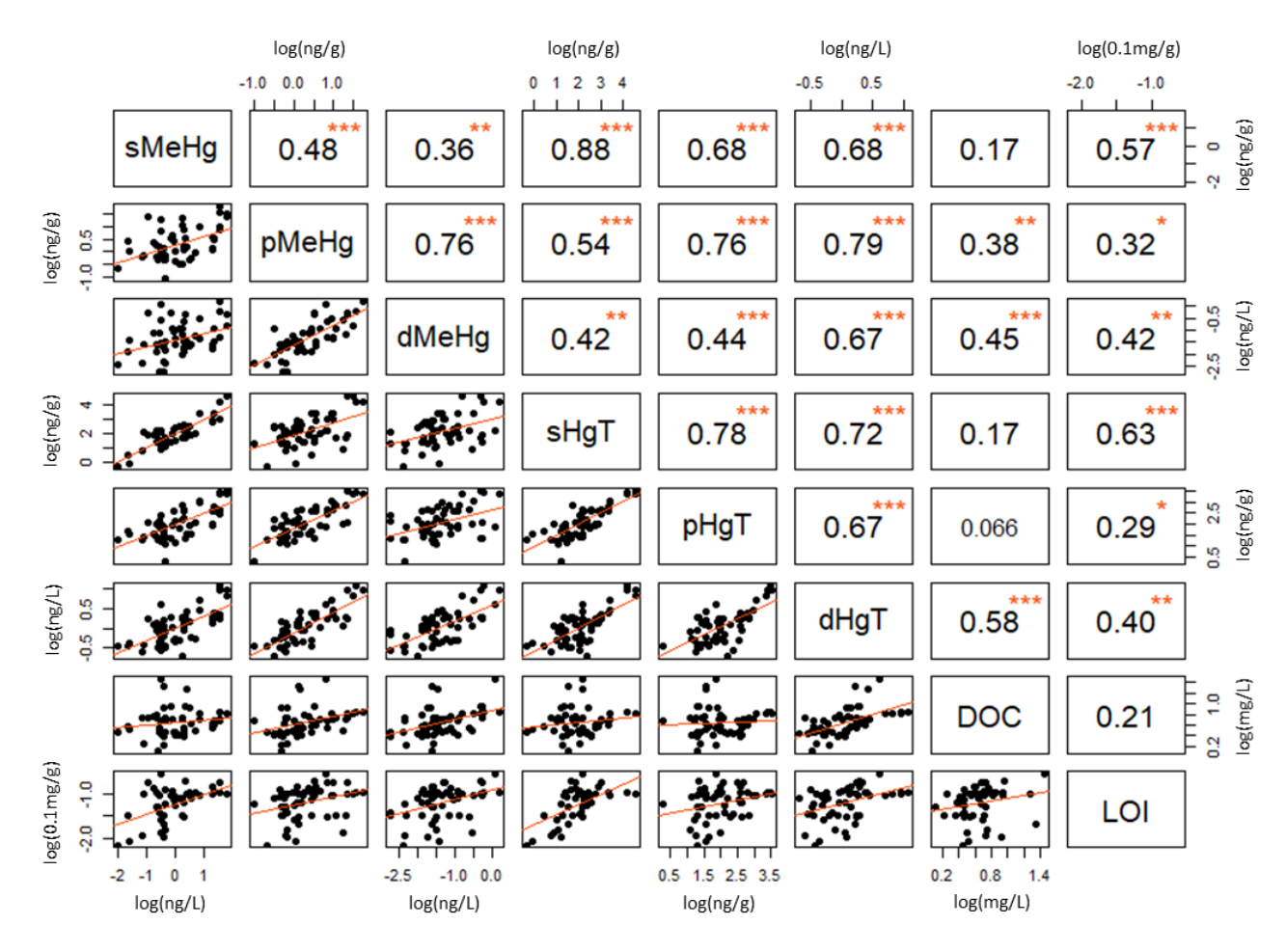


Figure 1. Full Model correlation matrix. The variable names are listed across the diagonals abbreviated as follows: methylmercury (MeHg), total Hg (HgT), bulk sediment (s-), particulate (p-), dissolved (d-), dissolved organic carbon (DOC), and % loss on ignition (LOI). In the lower left portion of the matrix the linear correlations are plotted. In the upper right portion of the matrix correlation coefficients are reported as well as symbols for significance as follows: <0.001= ***, 0.001-0.01= **, 0.01-0.05= *, 0.05-0.1= ., and >0.1= blank.

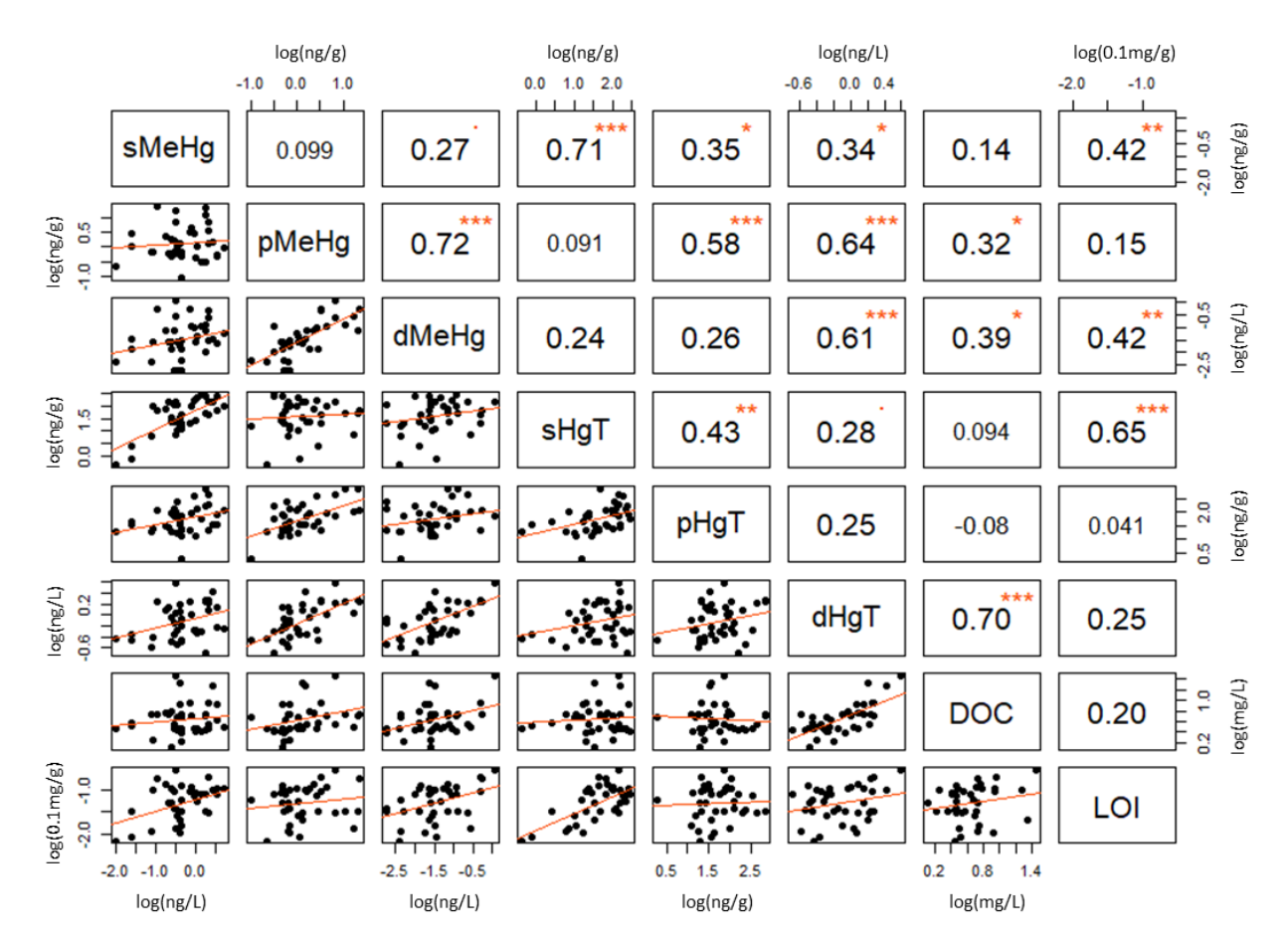


Figure 2. Reduced Model correlation matrix. The variable names are listed across the diagonals abbreviated as follows: methylmercury (MeHg), total Hg (HgT), bulk sediment (s-), particulate (p-), dissolved (d-), dissolved organic carbon (DOC), and % loss on ignition (LOI). In the lower left portion of the matrix the linear correlations are plotted. In the upper right portion of the matrix correlation coefficients are reported as well as symbols for significance as follows: <0.001= ***, 0.001-0.01= ***, 0.01-0.05= *, 0.05-0.1= ., and >0.1= blank.

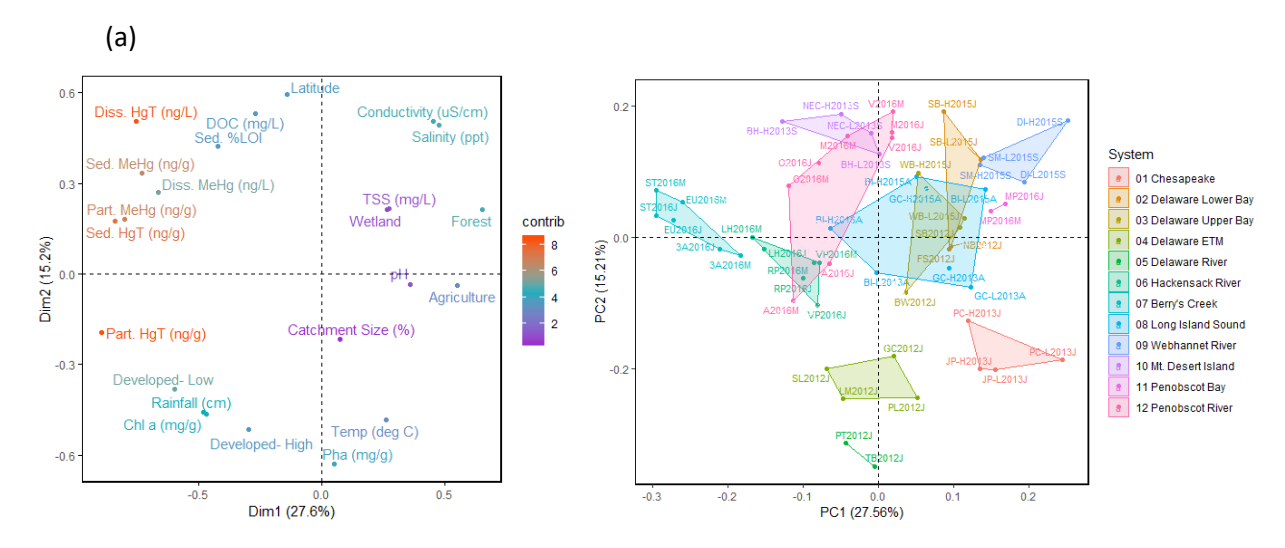


Figure 3. Plots of the first and second principal components derived from a principal component analysis of the Full dataset. Variables are plotted based on the correlation between each variable and components (a). The individuals (sites) are plotted based on their PC loadings (b). Each estuarine system is represented by a color as indicated in the legend, and each site is labelled on the plot.

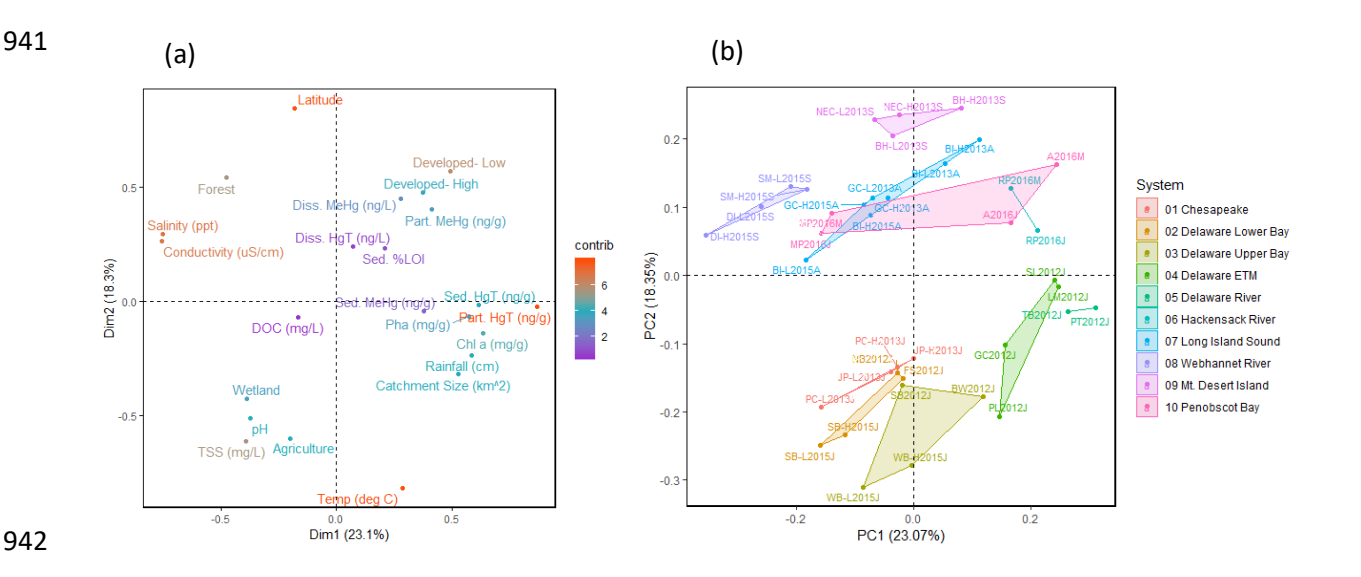


Figure 4. Plots of the first and second principal components derived from a principal component analysis of the Reduced dataset. Variables are plotted based on the correlation between each variable and components (a). The individuals (sites) are plotted based on their PC loadings (b). Each estuarine system is represented by a color as indicated in the legend, and each site is labelled on the plot.

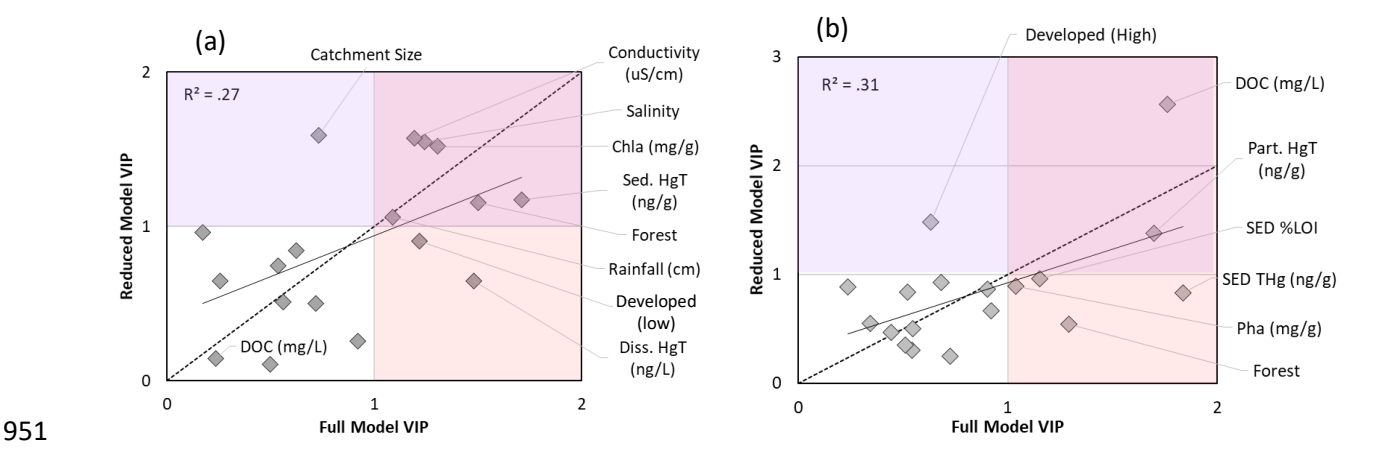


Figure 5. Variable Influence on the Projection (VIP) scores for a) the particulate HgT and b) the dissolved HgT Full Model versus the Reduced Model with the contaminated sites removed. VIP scores greater than one are considered important; variables with VIP scores greater than one in both models fall in the upper right, red quadrant whereas those that are important only in the full model fall in the lower right, orange quadrant and those that only important in the reduced model fall in the upper left, purple quadrant. A 1:1 line is plotted as a dashed line, and the linear

regression relationship is plotted as a solid line.

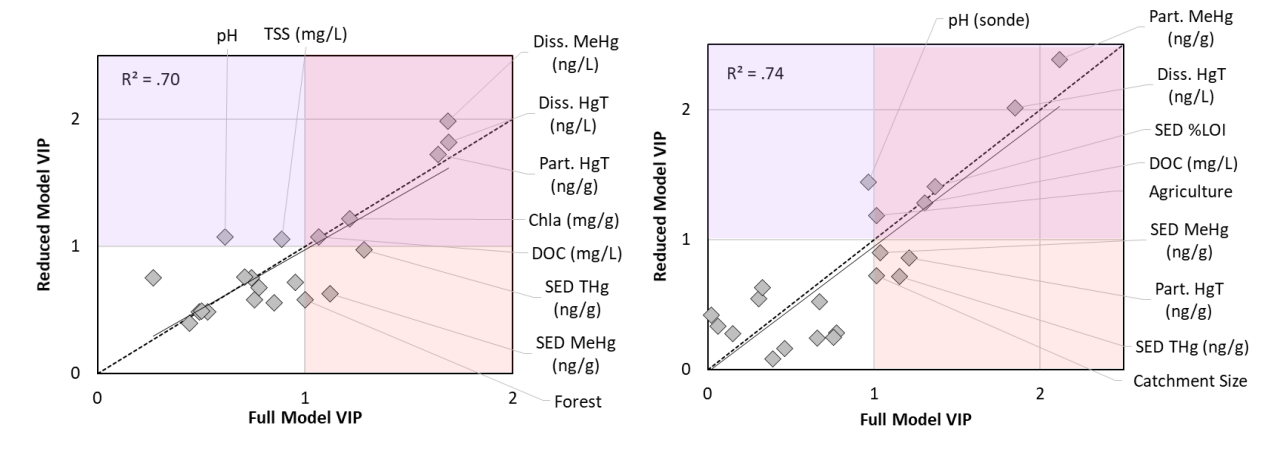


Figure 6. Variable Influence on the Projection (VIP) scores for a) the particulate and b) the dissolved MeHg Full Model versus the Reduced Model with the contaminated sites removed. VIP scores greater than one are considered important; variables with VIP scores greater than one in both models fall in the upper right, red quadrant whereas those that are important only in the full model fall in the lower right, orange quadrant and those that only important in the reduced model fall in the upper right-left, purple quadrant. A 1:1 line is plotted as a dashed line, and a linear regression relationship is plotted as a solid line.

Table 1. Site details including where and when each sample was collected.

State	System	Site Name	Subsite	Site	Month	Year	Latitude	Longitude
DE	Delaware River	North Beach		Code NB	July	2012	39.13	-74.89
DE	Delaware River	Fortescue		FS	July	2012	39.22	-74.83
DE	Delaware River	Sea Breeze		SB	July	2012	39.32	-75.32
DE	Delaware River	Buttonwood		BW	July	2012	39.46	-75.52 -75.51
DE	Delaware River	Pennsville Landfill		PL	July	2012	39.64	-75.55 -75.55
		S. of Lukens						-75.55 -75.55
DE	Delaware River			SL	July	2012	39.67	
DE	Delaware River	Luken's Marsh		LM	July	2012	39.69	-75.54
DE	Delaware River	Gen Chem		GC	July	2012	39.80	-75.44
DE	Delaware River	Timber Blvd		TB	July	2012	39.88	-75.13
DE	Delaware River	Penn Treaty		PT	July	2012	39.97	-75.13
MD	Chesapeake	Jefferson Patterson	HOC	JP-H	July	2013	38.39	-76.51
MD	Chesapeake	Jefferson Patterson	LOC	JP-L	July	2013	38.39	-76.51
MD	Chesapeake	Parker's Creek	HOC	PC-H	July	2013	38.54	-76.53
MD	Chesapeake	Parker's Creek	LOC	PC-L	July	2013	38.54	-76.52
СТ	Long Island Sound	Goshen	LOC	GC-L	August	2013	41.30	-72.12
CT	Long Island Sound	Goshen	HOC	GC-H	August	2013	41.31	-72.12
CT	Long Island Sound	Barn Island	LOC	BI-L	August	2013	41.34	-71.88
CT	Long Island Sound	Barn Island	HOC	BI-H	August	2013	41.34	-71.87
ME	Mt. Desert Island	Bass Harbor	LOC	BH-L	September	2013	44.25	-68.35
ME	Mt. Desert Island	Bass Harbor	HOC	ВН-Н	September	2013	44.25	-68.34
ME	Mt. Desert Island	Northeast Creek	HOC	NEC-H	September	2013	44.42	-68.33
ME	Mt. Desert Island	Northeast Creek	LOC	NEC-L	September	2013	44.43	-68.33
DE	Delaware River	Slaughter Beach	LOC	SB-L	July	2015	38.93	-75.31
DE	Delaware River	Cedar Creek	HOC	SB-H	July	2015	38.95	-75.32
DE	Delaware River	Duck Creek	HOC	WB-H	July	2015	39.33	-75.48
DE	Delaware River	Woodland Beach	LOC	WB-L	July	2015	39.33	-75.47
CT	Long Island Sound	Goshen Cove	HOC	GC-H	August	2015	41.31	-72.12
CT	Long Island Sound	Barn Island	LOC	BI-L	August	2015	41.34	-71.88
СТ	Long Island Sound	Barn Island	НОС	BI-H	August	2015	41.34	-71.87
ME	Webhannet River	Sea Mist	НОС	SM-H	September	2015	43.29	-70.58
ME	Webhannet River	Sea Mist	LOC	SM-L	September	2015	43.30	-70.58
ME	Webhannet River	Drake's Island	LOC	DI-L	September	2015	43.32	-70.56
ME	Webhannet River	Drake's Island	НОС	DI-H	September	2015	43.33	-70.56
NJ	Hackensack River	Veteran's Park		VP*	July	2016	40.67	-74.13
NJ	Hackensack River	Veteran's Park		VP*	May	2016	40.67	-74.13
NJ	Hackensack River	Rutkowski Park		RP	July	2016	40.69	-74.11
NJ	Hackensack River	Rutkowski Park		RP	May	2016	40.69	-74.11
NJ	Hackensack River	Laurel Hill		LH*	July	2016	40.76	-74.09
NJ	Hackensack River	Laurel Hill		LH*	May	2016	40.76	-74.09
NJ	Berry's Creek	Route 3 Underpass		3A*	July	2016	40.81	-74.09
147	Derry 3 Creek	Modic 5 Officer pass		5 A	July	2010	40.01	7 7.03

NJ	Berry's Creek	Route 3 Underpass	3A*	May	2016	40.81	-74.09
NJ	Berry's Creek	East Union	EU*	July	2016	40.82	-74.09
NJ	Berry's Creek	East Union	EU*	May	2016	40.82	-74.09
NJ	Berry's Creek	Stiletto's	ST*	July	2016	40.83	-74.08
NJ	Berry's Creek	Stiletto's	ST*	May	2016	40.83	-74.08
ME	Penobscot Bay	Moose Point	MP	July	2016	44.43	-68.94
ME	Penobscot Bay	Moose Point	MP	May	2016	44.43	-68.94
ME	Penobscot River	Verona	V*	July	2016	44.57	-68.79
ME	Penobscot River	Verona	V*	May	2016	44.57	-68.79
ME	Penobscot River	Marsh	M*	July	2016	44.59	-68.86
ME	Penobscot River	Marsh	M*	May	2016	44.59	-68.86
ME	Penobscot River	Orrington	0*	July	2016	44.69	-68.82
ME	Penobscot River	Orrington	0*	May	2016	44.69	-68.82
ME	Penobscot River*	Above	А	July	2016	44.76	-68.80
ME	Penobscot River*	Above	Α	May	2016	44.76	-68.80

^{*}Contaminated sites excluded from the Reduced Model

[†]Considered the Penobscot Bay in the Reduced Model